


Super-bound states in the continuum through merging in grating

Evgeny Bulgakov ¹, Galina Shadrina ², Almas Sadreev ^{1,*} and Konstantin Pichugin¹

¹*Kirensky Institute of Physics, Federal Research Center KSC SB RAS, 660036 Krasnoyarsk Russia*

²*Russia Institute of Computational Modelling SB RAS, 660036 Krasnoyarsk, Russia*

 (Received 5 June 2023; revised 28 August 2023; accepted 29 August 2023; published 14 September 2023)

We consider bound states in the continuum (BICs) in grating composed of infinitely long silicon rods of rectangular cross-section. We reveal merging off- Γ Friedrich-Wintgen BIC with symmetry protected BIC. We present CMT and multipole decomposition theory, complementing each other, to analyze the merging phenomenon. The theories show a crossover of the behavior of Q factor from standard inverse square law $k_{x,z}^{-2}$ towards extremely fast boosting law $k_{x,z}^{-6}$ in momentum space. In turn that crossover gives rise to another crossover from $Q \sim N^2$ to $Q \sim N^3$ for symmetry protected quasi-BIC in finite grating of N rods owing to suppression of radiation leakage of quasi-BIC mode from surface of grating. As a result, the Q factor of quasi-BIC is determined by residual leakage from ends of grating. We show numerically that this leakage can also be suppressed considerably if grating is stretched from the ends.

DOI: [10.1103/PhysRevB.108.125303](https://doi.org/10.1103/PhysRevB.108.125303)

I. INTRODUCTION

Comprehensively tailoring the resonant properties of electromagnetic resonators are of great importance in fundamental science and applications [1]. The quality (Q) factor of an electromagnetic resonator is a key indicator for numerous applications. In general, there are several effective ways to boost the Q factor, for example, whispering gallery modes in the cavities with convex smooth boundaries such as cylindrical, spherical, or elliptical cavities [2,3]. Another way is to use Fabry-Pérot resonator or hide the cavity in photonic crystals [1,4–6]. A fundamentally different approach involves the bound states in the radiation continuum (BICs), which provide unique opportunity to confine and manipulate electromagnetic wave within the radiation continuum [7–13]. The phenomenon of BICs is based on the fact that electromagnetic power can leak into only selected directions, which are given by diffraction orders, if dielectric cavities are arranged into periodical array [14–16]. Although the number of cavities N in the array can not be infinite, Q factor fastly grows with N quadratically for symmetry protected (SP) quasi-BICs [17–19] and cubically for accidental BICs [18,20,21]. However, all these predictions break down when the nonradiative loss $1/Q_{nr}$ of the photonic crystal (PhC) caused by material losses [19,21,22] and structural fluctuations [23,24] surpasses the radiative loss $1/Q_r$ of the system because of $1/Q = 1/Q_{nr} + 1/Q_r$. As a result, the nonradiative loss will impose an upper limit of Q_r factor in practice [19]. This pinpoints the importance of asymptotic behavior of the Q factor of BICs over the number of periods N , i.e., $Q_r(N) \sim N^\alpha$, because improving $Q(N)$ beyond Q_{nr} does not make any sense.

Therefore, exploring the ability to boost the Q factor approaching the upper bound set by the nonradiative loss becomes very important. It is therefore appealing to develop

feasible mechanisms for enlarging the asymptotic factor α . The last time the phenomenon of merging, at least, two BICs in momentum or parametric space [22,25–36] attracted much interest because of crossover of the index δ in the asymptotic behavior of the Q factor $Q_r \sim 1/(\text{parameter})^\delta$ from $\delta = 2$ towards $\delta = 6$ where both momentum space or geometrical dimensions of resonators can act as a parameter. In turn, merging of BICs forms a super-BIC [22,25,37]. In Ref. [38] the condition is derived according to which SP BIC in any symmetric 2D structure with 1D periodicity is the super-BIC exhibiting Q factor with degree $\delta = 6$. To the best of our knowledge there were no theory, which could show the mechanism of the crossover in the momentum space for merging BICs. Following to Ref. [22] we present in this paper two alternative theories complementing each other based on a generic two band effective non-Hermitian Hamiltonian (CMT theory) and multipole decomposition theory with application to grating. In the framework of the CMT theory we deduce a crossover of the index δ from 2 towards 6 for approaching merging point that completely agrees with the results of the multipole decomposition theory. In the framework of the latter theory we show the crossover is the result of full suppression of radiation from surface of grating. This result plays a key role for a crossover of asymptotic behavior of Q factor from $Q \sim N^2$ to $Q \sim N^3$ for finite grating. Along with that we offer a means suppress radiation from the ends by stretching grating that considerably boosts Q factor. The specific grating system is constituted of silicon rods of rectangular cross section as sketched in Fig. 1. This provides a parametric space for searching of merging BICs over aspect ratio of rods and wave vectors k_x or k_z . These two wave vectors define eigenfrequency bands in the PhC, avoiding the crossing of resonances (ACR), which gives rise to the FW off- Γ BIC along the symmetry momenta axis k_x or k_z . Moreover due to the symmetry of grating each band holds robust SP BICs at Γ point. Then for variation of cross section of rods we observe merging FW BIC and SP BIC.

*Corresponding author: almas@tnp.krasn.ru

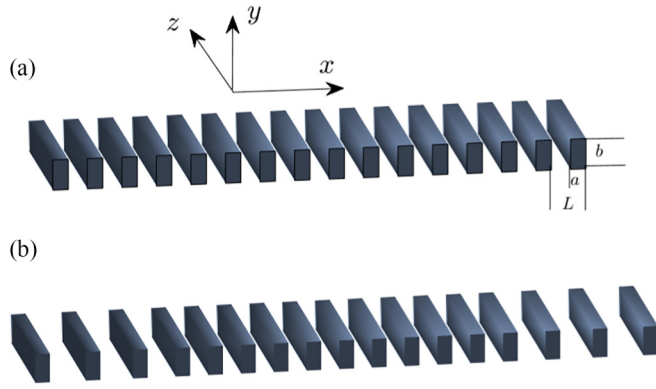


FIG. 1. Two cases of gratings. (a) With the constant period L and (b) stretched from the ends. The dielectric permittivity of rods in air $\epsilon = 12.11$.

II. NUMERICS FOR ACR OF EIGENFREQUENCY BANDS IN GRATING AND MERGING BICS

An interesting feature of open dielectric cavity is that variation in its shape leads to its real parts of complex

eigenfrequencies (resonant frequencies) undergoing ACR accompanied by strong redistribution of the imaginary parts of the complex eigenfrequencies. As a result, the Q factor can be strongly enhanced [39–46] forming supercavity modes due to hybridization of resonant modes. All these features refer to the present system of array of rods for variation of the height of rods that is demonstrated in Fig. 2. Insets in Figs. 2(a) and 2(c) show hybridization of resonant eigenmodes owing to interaction through closed radiation diffraction continua.

A grating of infinitely long rods is specified by eigenfrequency bands, which can be clearly seen in transmittance of plane wave through the grating as Fig. 3 shows. Coupling of the eigenmodes with the radiation continuum leads to ACR of bands that in turn can give rise to Friedrich-Wintgen (FW) BICs beyond Γ point [14–16,47,48]. Also the bands can be featured by symmetry-protected BIC at Γ point owing to the symmetry mismatching of the corresponding eigenmode with the radiation continuum of the first diffraction channel [47,49–53]. All BICs are marked in Fig. 3 where evolution of mode profiles is shown in Figs. 2(a) and 2(c). Although ACR in Fig. 2 is given beyond Γ point, quite similar ACR takes place at the Γ point. Correspondingly mode profiles in Figs. 2(a) and 2(c) are very close to the true BICs. As marked by closed

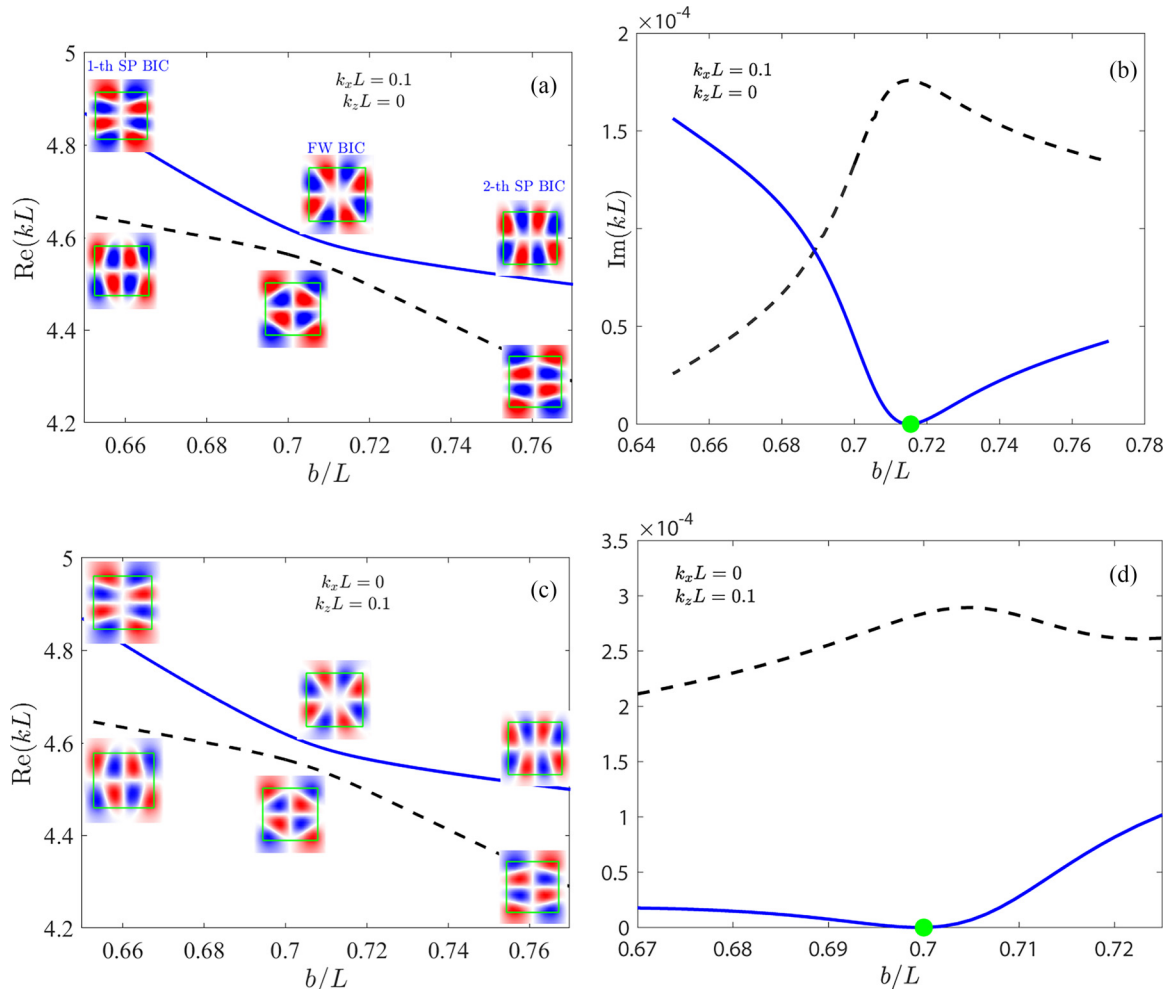


FIG. 2. ACR of two resonant modes vs height of rod b at $a/L = 0.75$ in the infinite grating. Insets of electric field $\text{Re}(E_z)$ illustrate hybridization of resonant modes for ACR. Green closed circles mark FW BICs. $kL = \omega L/c$ is the dimensionless frequency.

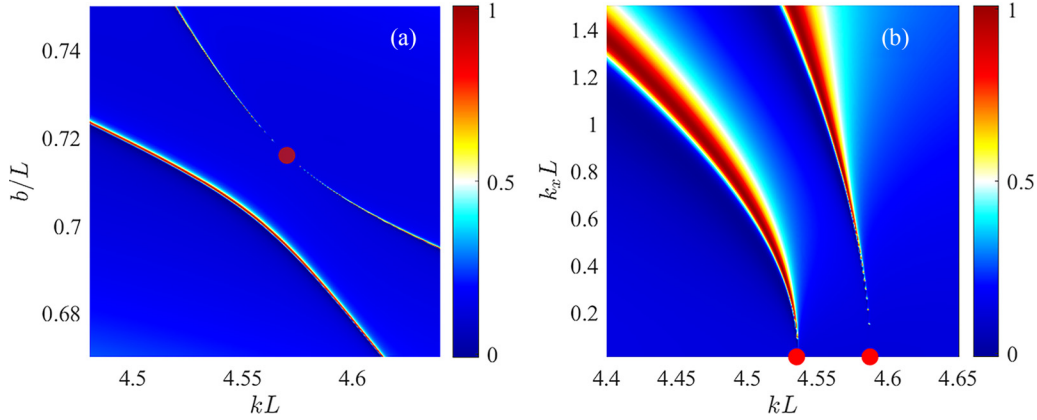


FIG. 3. (a) Transmittance of TM plane wave with electric field directed along z axis vs frequency and aspect ratio of rods at $k_x L = 0.25$, $k_z = 0$ where circle marks FW BIC. (b) Transmittance vs Bloch vector k_x at $b/L = 0.71$ and $k_z = 0$. Closed circles mark SP BICs at Γ points. $kL = \omega L/c$ is the dimensionless frequency.

circles in Figs. 2(b) and 2(d) FW BICs occur in both directions of momenta space.

In what follows we focus below on merging of BICs that constitute the most interesting and important phenomenon. In Fig. 4 we demonstrate as height b/L of silicon rods varies the off- Γ FW BIC merges with one of SP BIC at Γ point with $k_x \neq 0$ or $k_z \neq 0$. One can see an exceptionally high sensitivity of merging to the selection of b/L ratio. Figure 5 illustrates why the phenomenon of merging is of great importance because of strong crossover in the dependence of Q factor on wave vectors k_x at $k_z = 0$ and k_z at $k_x = 0$ from $Q \sim 1/k_x^2$, $1/k_z^2$ to $Q \sim 1/k_x^6$, $1/k_z^6$ as indicated by the insets, suggesting a limit to the merging points. Beyond merging point the Q factor can be approximated as

$$Q \sim \frac{1}{k_x^2(k_x - k_{x,BIC})^2(k_x + k_{x,BIC})^2}$$

as was derived by Jin *et al.* by symmetry arguments [25] and numerically by Hwang *et al.* [26] in 2D PhCs. Below we derive this dependence analytically based on alternative multipole decomposition theory. Note that similar dependence of Q factor on k_z as Fig. 5(b) shows. These results for merging

FW BIC and SP BIC are expressed as dependence of wave vectors on structural parameter b/L of rods in Fig. 6.

III. THE CMT THEORY OF MERGING AND SUPER-BICS

In order to qualitatively describe merging off- Γ FW BIC and SP BIC we introduce a generic two-level description of effective non-Hermitian Hamiltonian following Ref. [22],

$$H_{eff} = \begin{pmatrix} \varepsilon + ek_x^2 - i\gamma_1 k_x^2 & u - i\sqrt{\gamma_1 \gamma_2} k_x^2 \\ u - i\sqrt{\gamma_1 \gamma_2} k_x^2 & -\varepsilon - ek_x^2 - i\gamma_2 k_x^2 \end{pmatrix} + \lambda \begin{pmatrix} 1 & 0 \\ 0 & 1 \end{pmatrix}. \quad (1)$$

The matrix elements have clear physical origin. Real parts of diagonal elements respond to eigenfrequencies $\pm(\varepsilon + ek^2)$ of closed system with band structure, imaginary parts do for decay rates $\gamma_j k_x^2$, $j = 1, 2$ into open channel of radiation continuum for deviation from Γ point. Therefore at Γ point ($k_x = 0$) the Hamiltonian describes two SP BICs with correspondence to Fig. 3(b). Off-diagonal matrix elements are responsible for coupling of eigenmodes of closed system

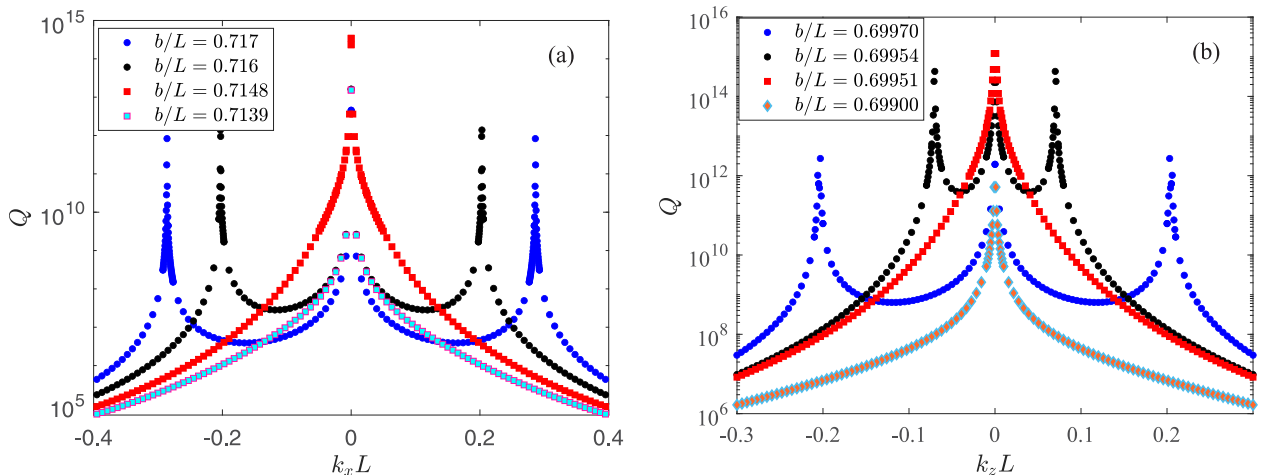
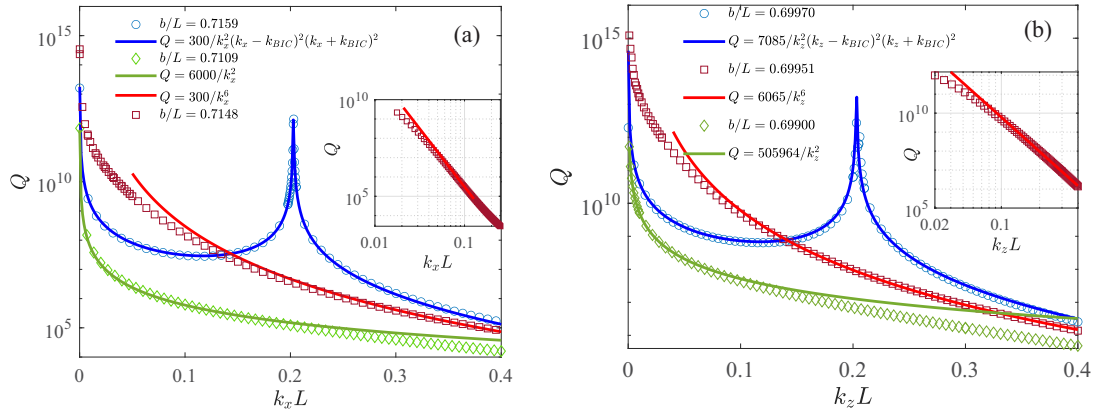


FIG. 4. Merging FW BIC and SP BIC over Bloch wave number k_x at $k_z = 0$ (a) and wave vector k_z at $k_x = 0$ (b).


 FIG. 5. Strong redistribution of Q factor on Bloch wave vector (a) and waveguide vector k_z (b) at merging.

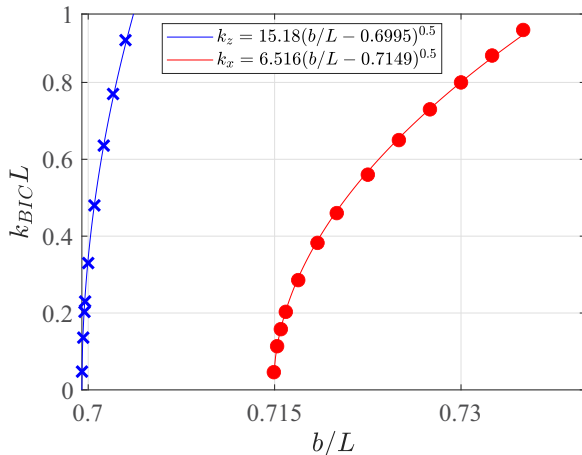
through open $\sqrt{\gamma_1 \gamma_2}$ and closed channels of the continuum u . The parameters $\varepsilon(b/L)$, $\lambda(b/L)$, and e are responsible to two PhC bands at Γ point. Although this Hamiltonian is widely used to describe FW BICs [54–56], it, however, holds important contribution for dispersive resonant eigenmodes of the grating. The quantitative values for all model constants in the Hamiltonian (1) can be extracted from numerically calculated complex eigenfrequencies of the grating and are given in Fig. 7 where a contribution of the trivial second part of unit matrix is disregarded.

The complex eigenfrequencies of the effective Hamiltonian (1)

$$Z_{1,2} = -i\gamma k_x^2 \pm \sqrt{(\varepsilon + ek_x^2 - i\delta\gamma k_x^2)^2 + (u - i\sqrt{\gamma_1 \gamma_2} k_x^2)^2} \quad (2)$$

describe two resonances whose imaginary parts or resonant widths versus ε , i.e., aspect ratio b/L and wave vector k_x as shown in Fig. 7. Here $\gamma = \frac{\gamma_1 + \gamma_2}{2}$, $\delta\gamma = \frac{\gamma_1 - \gamma_2}{2}$. At $k_x = 0$ the model describes two SP BICs for any ε in agreement with Fig. 3(b). Moreover the model describes also one off- Γ BIC of the Friedrich-Wintgen origin due to avoided crossing of two bands for specific k_x , which depends also on ε . That occurs at

$$\varepsilon = \tilde{u}\delta\gamma - ek_{x,BIC}^2, \quad (3)$$


 FIG. 6. The dependencies of momenta of FW BIC on a height b/L of rods at fixed width $a/L = 0.75$.

where $\tilde{u} = \frac{u}{\sqrt{\gamma_1 \gamma_2}}$. This equation follows from equation for FW BIC derived in Refs. [55–57]. Moreover, Eq. (3) predicts square dependence of the structural parameter $\varepsilon(b/L)$ on wave vector of FW BIC that completely agrees with numerics presented in Fig. 6.

However, what is most important is that Eq. (3) describes merging FW BIC with one of SP BIC at $\varepsilon = \tilde{u}\delta\gamma$ for $k_x \rightarrow 0$ as seen from Fig. 8(a). Beyond the merging point the imaginary parts of both resonant modes proportional to k_x^2 give inverse squared behavior ($\delta = 2$) of the Q factor as follows, from Eq. (2). At the merging point the eigenvalues (2) are

$$Z_{1,2} = -i\gamma k_x^2 \pm \gamma(\tilde{u} - ik_x^2) \times \sqrt{1 + \frac{2e\delta\gamma k_x^2}{\gamma^2(\tilde{u} - ik_x^2)} + \frac{e^2 k_x^4}{\gamma^2(\tilde{u} - ik_x^2)^2}}. \quad (4)$$

At the vicinity of Γ point, $k_x \ll 1$ we obtain the remarkable result of extremely large index $\delta = 6$ for resonant width at the merging point

$$Z_1 \approx -\gamma\tilde{u} - \frac{\delta\gamma e}{\gamma} k_x^2 - i\frac{a^2\gamma_1\gamma_2}{2\tilde{u}^2\gamma^3} k_x^6, \quad (5)$$

that is, the Q factor at the merging point grows as $1/k_x^6$. Thus, the Hamiltonian (1) describes the crossover of the quality factor $Q \sim 1/k_x^\delta$ from $\delta = 2$ towards $\delta = 6$. This analytical result agrees with numerical computation shown in Fig. 5(a) and explains numerical observations presented for 2D PhCs [25,26]. Obviously, a similar analytical result can be obtained for Q factor versus waveguide vector k_z in full agreement with our numerical computations presented in Fig. 5(b). In the next section we show that the crossover in suppression of leakage at merging BICs plays an important role in the crossover of asymptotic behavior of Q factor from N^2 to N^3 for quasi-SP BIC that justifies a terminology of super-BIC [26] in grating with finite number N of rods.

IV. MULTIPOLE DECOMPOSITION THEORY OF SUPPRESSION OF RADIATION AT MERGING DUE TO ACR

The definition of quality factor Q is the ratio of the energy stored in the system to the radiated power. We consider the

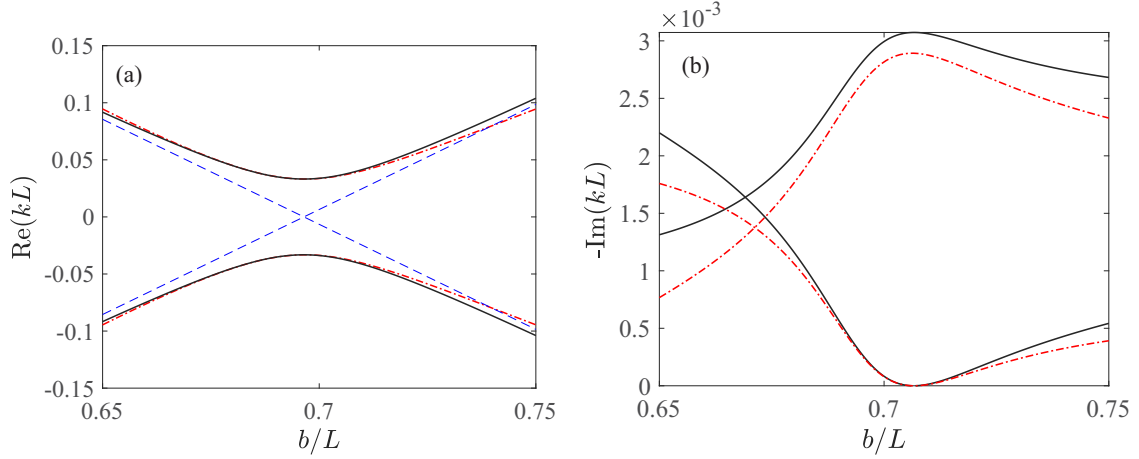


FIG. 7. Real (a) and imaginary (b) parts of two complex eigenvalues at $k_x L = 0.4, k_z = 0$. Solid lines show calculated numerically at $a/L = 0.75$ while dash-dotted lines show fitted behavior to result with $\varepsilon = -1.918b/L + 1.337, e = 0.027, \gamma_1 = 0.0143, \gamma_2 = 0.00487, u = 0.0336$.

high-refractive index rods and think that the internal energy stored in the rods is much greater than the external energy stored outside [58]. The radiation leakage can be evaluated via multipole decomposition of scattering function,

$$E_z(x, y) = \sum_j \sum_m a_m e^{ij k_x L} H_m(k r_j) e^{im \phi_j}, \quad (6)$$

where j runs over rectangular rods as sketched in Fig. 9. Here r_j and ϕ_j are the polar coordinates of the j th radius vector, and $\mathbf{r}_j = \mathbf{r} - jL\mathbf{e}_x$.

Using a relationship between the cylindrical harmonic fields and the space-harmonic fields [59], we have for scattering field

$$E_z(x, y) = \sum_m a_m \frac{2(-i)^m}{L k^m} \sum_{n=-\infty}^{\infty} \frac{(k_{x,n} + i k_{y,n})^m}{k_{y,n}} \times e^{i k_{x,n} x + i k_{y,n} y}, \quad y > 0, \quad (7)$$

where

$$k_{x,n} = k_x + \frac{2\pi n}{L}, k_{y,n} = \sqrt{k^2 - k_{x,n}^2}, \quad (8)$$

and integers $n = 0, \pm 1, \pm 2, \dots$ enumerate diffraction orders, i.e., radiation continua. In what follows we consider SP BICs embedded into the first continuum $n = 0$ with the eigenfrequency of BICs $k < 2\pi/L$. The scattering field (7) in the far zone can be approximated as

$$E_z(x, y) \approx \frac{2}{L k \cos \theta} \sum_m a_m(k_x) e^{-im\theta} \times e^{i k_x x + i k_y y} = F e^{i k_x x + i k_y y}, \quad y > 0, \quad (9)$$

where $k_x = k \sin \theta, k_y = k \cos \theta$. Since the scattering function (7) is odd relative to $x \rightarrow -x$ we have $a_{2m}(k_x) = -a_{-2m}(k_x), a_{2m+1}(k_x) = a_{-2m-1}(k_x)$. Moreover, $a_{2m}(k_x) = a_{2m}(-k_x), a_{2m+1}(k_x) = -a_{2m+1}(-k_x)$. We thus have from

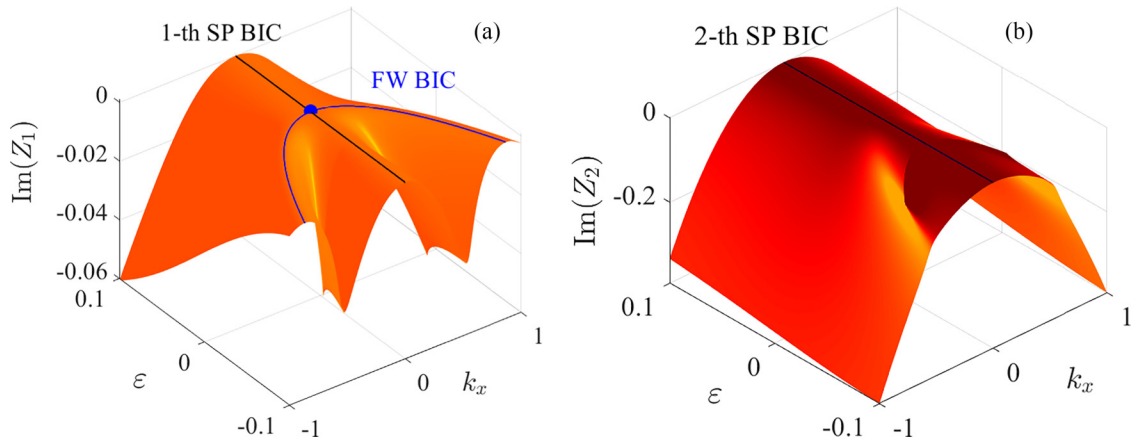


FIG. 8. [(a),(b)] The imaginary parts of two complex eigenvalues (2) of the effective Hamiltonian (1) with two SP-BICs and one off- Γ FW BIC. Solid lines show SP and off- Γ FW BIC given by Eq. (3). Closed circle marks merging point. The parameters of Hamiltonian (1) are chosen as follows: $e = 0.15, \gamma_1 = 0.3, \gamma_2 = 0.1, u = 0.02$.

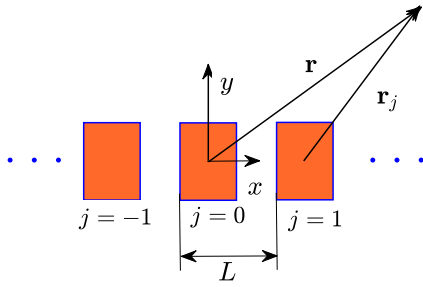


FIG. 9. Infinite periodical array of rectangular rods.

Eq. (9),

$$F = \frac{4}{Lk \cos \theta} \left[-i \sum_{m=1}^{\infty} a_{2m}(k_x) \sin(2m\theta) + \sum_{m=0}^{\infty} a_{2m+1}(k_x) \cos((2m+1)\theta) \right]. \quad (10)$$

For slight deviation from the merging point, i.e., for small $\theta \approx k_x/k = \xi \ll 1$ we have the following approximate series: $\sin \xi \approx \xi - \xi^3/6$, $\cos \xi \approx 1 - \xi^2/2$. Moreover we write the series for the amplitudes $a_{2m}(\xi) \approx a_{2m}(0) + a''_{2m}(0)\xi^2/2$, $a_{2m+1}(\xi) \approx a'_{2m+1}(0)\xi + a'''_{2m+1}(0)\xi^3/6$. A substitution of all these series into Eq. (10) gives us

$$F \approx P_1 k_x + P_3 k_x^3, \quad (11)$$

with accuracy of cubic contribution k_x^3 . Thus, we have for the Q factor, which is a ratio of stored energy U and leaking power $W = |F|^2$,

$$Q = \frac{kU}{|F|^2} = \frac{kU}{|P_1 k_x + P_3 k_x^3|^2}, \quad (12)$$

where

$$P_1 = -\frac{4i}{k^2 L} \left[\sum_{m=1}^{\infty} 2ma_{2m}(0) + ik \sum_{m=0}^{\infty} \frac{da_{2m+1}(0)}{dk_x} \right] = -\frac{4i}{k^2 L} P. \quad (13)$$

In what follows we are mainly interested in qualitative behavior of Q factor over momentum k_x near merging point. Thereby we can omit the cumbersome expression for P_3 that has no effect on crossover and therefore can be substituted simply as complex constant C slightly independent of k_x . The only importance is that the expression P_1 turns to zero owing to merging BICs while the expression P_3 does not, as Comsol Multiphysics calculations illustrate in Fig. 10.

Also Fig. 10 shows that P_1 turns to zero at merging point with accuracy of numerical errors.

Moreover we present in Fig. 10 the first two decomposition coefficients $a_2(0)$ and $a_4(0)$ calculated via integrals over cross section of rods [60],

$$a_m = \frac{i\pi k^2}{2} \int d\Omega J_m(kr) \frac{e^{-im\phi}}{\sqrt{2\pi}} (\epsilon(\mathbf{x}) - 1) E_z^*(\mathbf{x}) d\Omega. \quad (14)$$

One can see that $a_2(0)$ undergoes critical behavior owing to ACR through which the lowest contribution in multipole radiation P_1 turns to zero in accordance with Eq. (13).

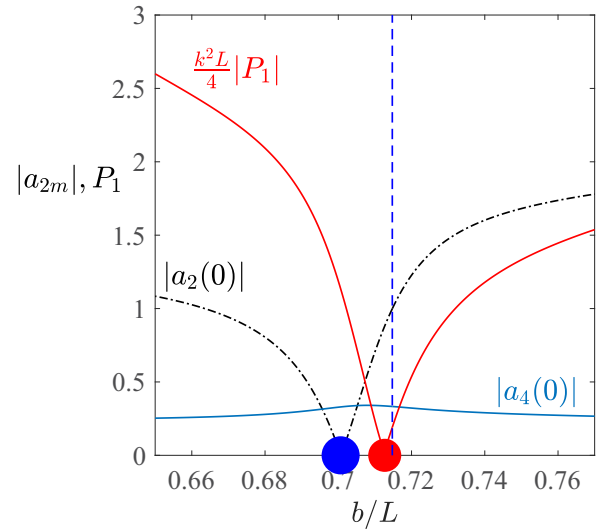


FIG. 10. Behavior of the first two decomposition coefficients $a_2(0)$, $a_4(0)$ and the magnitude P_1 in Eq. (13) vs aspect ratio of rods b/L . Dash line corresponds to merging point.

In view of last considerations we present the coefficients in Eq. (12) as

$$P_1 = \beta(b - b_c), \quad P_3 = C, \quad (15)$$

where b is the structural parameter shown in Fig. 1. As a result we obtain

$$Q \sim \frac{1}{|\beta(b - b_c)k_x + Ck_x^3|^2}. \quad (16)$$

Thus, for infinite grating we obtain that Q factor turns to infinity, i.e., BIC

$$k_x^2 = \frac{\beta}{C}(b_c - b). \quad (17)$$

Rigorously speaking this equation gives us complex momentum k_x . However, in order for the Bloch BIC solution $\exp(ik_x x)$ to be meaningful we have to take that both complex constants have the phase difference equal to zero or π . As Fig. 6 shows the phase difference equals to π to give

$$k_x^2 = \frac{|\beta|}{|C|}(b - b_c). \quad (18)$$

Thus, at the merging point $b = b_c$ we have

$$Q \sim \frac{1}{k_x^6}. \quad (19)$$

It is remarkable, from Eq. (16) we have

$$Q \sim \frac{1}{k_x^2 | -\beta(b - b_c) + Ck_x^2 |^2} = \frac{1}{\beta k_x^2 (k_x + k_{BIC})^2 (k_x - k_{BIC})^2}, \quad (20)$$

where $k_{BIC} = \sqrt{\beta(b - b_c)/C}$ that fully agrees with numerical derivations presented in Fig. 5 as well as with numerically derived expressions by Jin *et al.* [25] for 2D PhC.

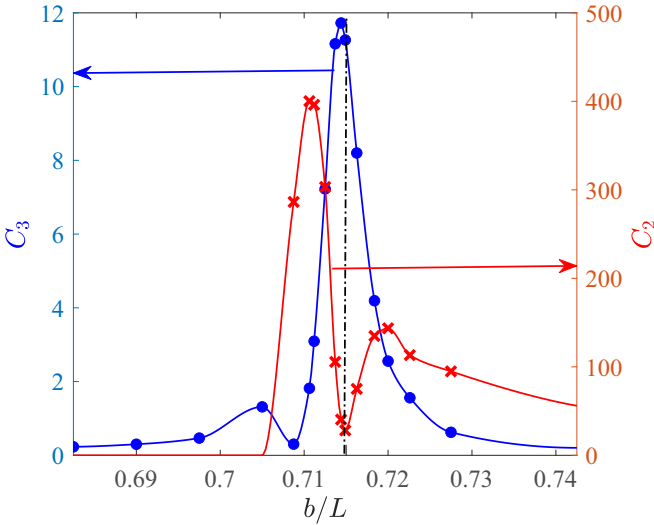


FIG. 11. Behavior of coefficients C_2 (right) and C_3 (left) in dependence of the Q factor $Q = C_2N^2 + C_3N^3$ vs the number of rods in grating N . Closed circles and crosses show Comsol calculations, solid lines show interpolation at the interval of $N = 10$ till $N = 100$. Dashed line corresponds to merging point.

Now we consider grating with finite number of rods N and argue that a change of the index δ in asymptotical behavior of the $Q \sim \frac{1}{k_x^\delta}$ for merging BICs results in the change of the behavior of Q factor over the number of resonators from quadratic to cubic. We assume that the EM power radiates from surface of finite grating, which has the same origin as leakage calculated above and from the ends of grating, thus we have for the quality factor [17]

$$\frac{1}{Q} = \frac{1}{Q_\perp} + \frac{1}{Q_\parallel}. \quad (21)$$

Here the first contribution Q_\perp is the contribution of quasi-SP BIC, which is a standing wave with the wave number $k_x = \pi/NL$ [17,19]. Therefore aside radiation from the surface of

finite grating gives us

$$\frac{1}{Q_\perp} \sim \frac{D_2}{N^2} + \frac{D_6}{N^6}, \quad (22)$$

according to Eq. (12) in agreement with the above derivations of crossover at a vicinity of merging. At the merging point the first contribution vanishes to become negligibly small compared to radiation from the ends of finite grating to write $D_2 \sim |b - b_c|$. It was already derived that $Q_\parallel \sim N^3$ by use of the tight-binding approximation [20,61–63]. The crossover can be traced in numerics by fitting $Q = C_2N^2 + C_3N^3$ in the interval for N from 10 till 100 as Fig. 11 illustrates.

Therefore at merging SP BIC and FW off- Γ BIC we obtain crossover for Q factor from $Q \sim N^2$ to $Q \sim N^3$ resulting in super-quasi-BIC as Comsol MultiPhysics calculations illustrate in Fig. 12.

Moreover we employ an additional method to considerably boost the Q factor by adjustment of additional buffer gratings to the ends of grating [62,64–67]. These buffer grating have either the period L_b slightly different from the period L of basic grating or the period of buffer gratings gradually stretching as sketched in Fig. 1(b) and shown in Fig. 13. That gives rise to strong suppression of the wave function near the ends of grating as shown in Figs. 13 and 14. Moreover Fig. 13 demonstrates crucial enhancement of Q factor owing to stretching at merging point caused by suppression of radiation from ends of grating. One can see that in spite of very small stretching of grating we observe suppression of wave function at the ends of finite gratings. As a result we have strong boosting of the Q factor for increasing the period of grating by 1% at merging as Comsol MultiPhysics simulations of Q factor show in Fig. 15. One can also see from this figure that Q factor is boosting much stronger at the merging because of suppression of surface radiation while radiation from the ends is suppressed by stretching.

In both cases the effect of suppression of radiation from the ends of grating originates from quantum tunneling through potential barrier [62]. Consider SP BIC at Γ point shown by closed red circles in Fig. 3(b), which are positioned at bottoms of frequency bands. In finite grating of N rods with period L this BIC transfers into quasi-BIC. Assume that two auxiliary

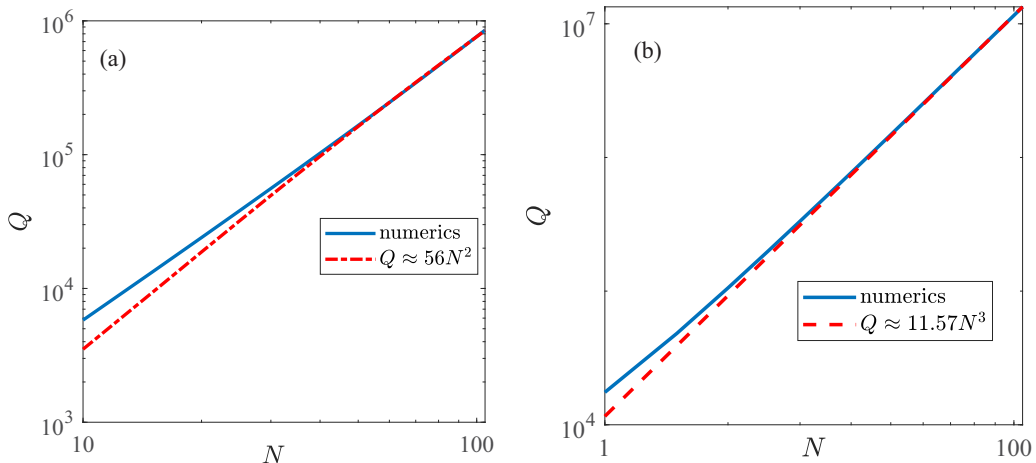


FIG. 12. Dependence of the Q factor on the number of rods in finite grating. (a) Far from merging point at $b = 0.7425L$ and (b) at merging $b/L = b_c/L = 0.7148$, $a/L = 0.75$.

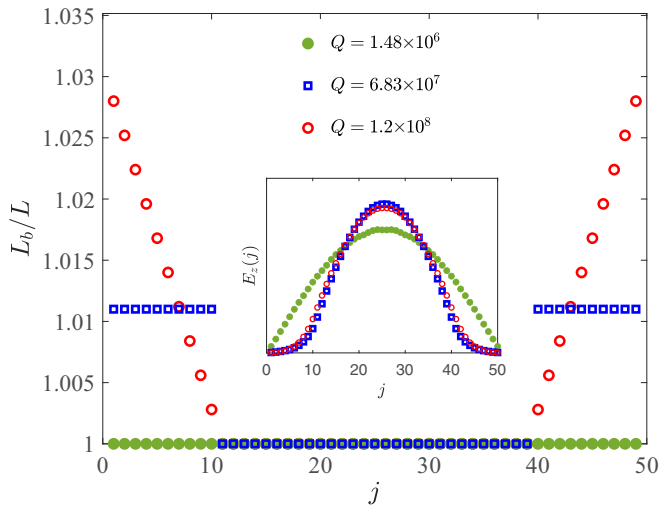


FIG. 13. The periods between rods $L_b(j)$ of buffer gratings in terms of the constant period of inner grating L . Inset shows maximal values of mode amplitudes $E_z(j) = \max(|E_z(x, y)|)$ inside j th rod.

gratings of N_b rods with the period L_b are attached to ends of primary grating. For $L_b > L$ the bands in the auxiliary gratings descend by $\Delta \approx (L_b - L)/L$ relative to the bands in primary grating. For the specific case in Fig. 13 we obtain numerically $e = -0.047$, $\Delta = 0.012$, the shift of bottom of frequency band equals -0.705Δ . Therefore the frequency of quasi-SP BIC of primary grating, which is close to zero will enter the bandgap of auxiliary grating at point $0.705\Delta - ek_x^2 = 0$. Hence the solution of BIC in bandgap of auxiliary grating decays as $\exp(ik_x L_b N_b) = \exp(-\sqrt{0.705\Delta/e} L_b N_b)$. Inverse of this exponential factor defines boosting of Q factor by a value of $1/0.014 \approx 71$ times. As far as the grating stretched linearly from the ends shown in Fig. 1(b) the physical mechanism of suppression of radiation from the ends is similar. Simple qualitative estimations given above are applicable, however, with correction related to asymptotic behavior of the Eiry solution.

V. SUMMARY

We developed a concept of super-BIC [25,27,37] as a result of merging “usual” Friedrich-Wintgen off- Γ BIC with SP BIC

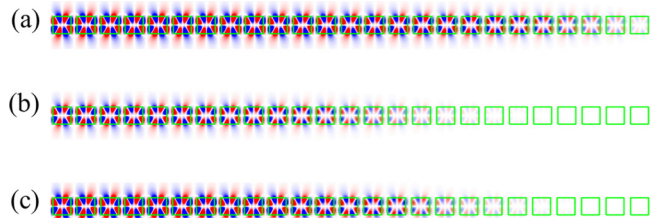


FIG. 14. (a) The profiles of the solutions ($\text{Re}[E_z(x, y)]$) in finite gratings with the constant period L , the grating is shielded by two gratings with the period $L_b/L = 1.015$ (b) as shown by squares in Fig. 13, and the grating is gradually stretched from the ends (c) as shown by open circles in Fig. 13. Because of symmetry only the half of mode profiles are shown.

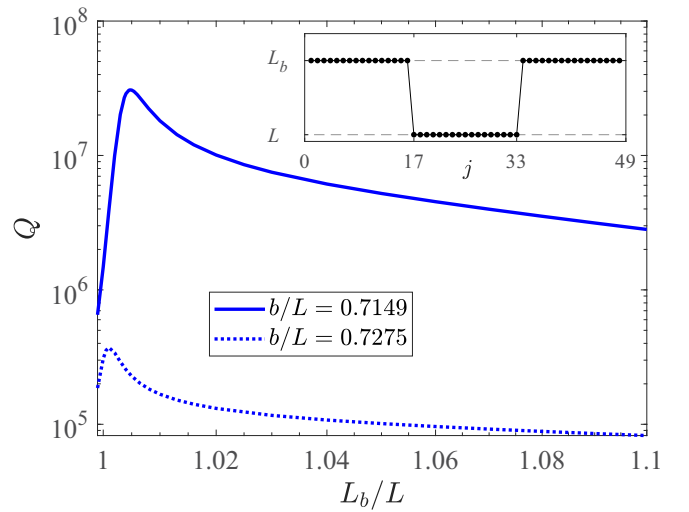


FIG. 15. Q factor of buffered grating vs period of buffers. Solid line corresponds to the merging point while dotted line does beyond merging point.

at Γ point in the case of grating constituted of silicon rods of rectangular cross section. The merging phenomenon reported recently in application to different systems [22,26,27,29–31,33–36] has attracted much interest because of crossover of asymptotic behavior of Q factor over critical parameter. Wave vector, which defines frequency bands in PhCs attracts particular interest as this parameter because of importance of the merging applied to real finite photonic systems of finite size LN where L is the period and N is the number of elementary cells. The smallest value of wave vector π/LN responsible for quasi-SP BIC defines the asymptotical behavior of Q_{\perp} factor over N of the quasi-BIC mode because of leakage from surface of grating [17,19]. We presented an analytical theory based on multipole decomposition of this radiation loss. For merging of FW off- Γ BIC and SP BIC at Γ point for limiting of the wave vector to zero a surface radiation is completely suppressed leaving smaller radiation from the ends of finite grating, which decreases with the number of rod as $1/N^3$ [20,61–63]. That transforms asymptotical behavior of Q factor from standard law $k_{x,z}^{-2}$ to superhigh Q factor behavior $k_{x,z}^{-6}$ that justifies it to be termed super-BIC [25,27,37,68]. Thus for finite grating we obtain the crossover of Q factor from standard square law N^2 towards cubic one N^3 . Moreover, Jun [25] first established link between topological charge of BIC and critical index for $Q \propto 1/k_{x,z}^{2\delta}$ in 2D PhCs with symmetries C_{4v} and C_{6v} . It was shown that the degree δ is increased for annihilation of nine [25] and five [69] topological charges.

In addition, we presented a simple analytical theory based on a generic non-Hermitian effective Hamiltonian (CMT model) accounting for two frequency bands of PhC, which explains all the above-described phenomena. Our approach constitutes an important difference compared to Ref. [70] in which CMT theory was explored to consider ACR of two off- Γ BICs. Owing to generic form of Hamiltonian (1) the

model is applicable to arbitrary PhC system in which merging of BICs was observed [22,25–27]. The theory completely agrees with multipole decomposition theory and numerical Comsol Multiphysics results.

ACKNOWLEDGMENTS

We thank Yi Xu and Zhanyuan Zhang for numerous fruitful discussions. The work was supported by Russian Science Foundation Grant No. 22-12-00070.

-
- [1] K. J. Vahala, Optical microcavities, *Nature (London)* **424**, 839 (2003).
- [2] V. Braginsky, M. Gorodetsky, and V. Ilchenko, Quality-factor and nonlinear properties of optical whispering-gallery modes, *Phys. Lett. A* **137**, 393 (1989).
- [3] M. L. Gorodetsky and V. S. Ilchenko, Optical microsphere resonators: Optimal coupling to high-Q whispering-gallery modes, *J. Opt. Soc. Am. B* **16**, 147 (1999).
- [4] J. D. Ryckman and S. M. Weiss, Low mode volume slotted photonic crystal single nanobeam cavity, *Appl. Phys. Lett.* **101**, 071104 (2012).
- [5] P. Seidler, K. Lister, U. Drechsler, J. Hofrichter, and T. Stifferle, Slotted photonic crystal nanobeam cavity with an ultrahigh quality factor-to-mode volume ratio, *Opt. Express* **21**, 32468 (2013).
- [6] J. Zhou, J. Zheng, Z. Fang, P. Xu, and A. Majumdar, Ultra-low mode volume on-substrate silicon nanobeam cavity, *Opt. Express* **27**, 30692 (2019).
- [7] C. W. Hsu, B. Zhen, S.-L. Chua, S. G. Johnson, J. D. Joannopoulos, and M. Soljačić, Bloch surface eigenstates within the radiation continuum, *Light: Sci. Appl.* **2**, e84 (2013).
- [8] S. I. Azzam and A. V. Kildishev, Photonic bound states in the continuum: From basics to applications, *Adv. Opt. Mater.* **9**, 2001469 (2020).
- [9] L. Huang, L. Xu, M. Woolley, and A. Miroshnichenko, Trends in quantum nanophotonics, *Adv. Quantum Tech.* **3**, 1900126 (2020).
- [10] Z. Hu, L. Yuan, and Y. Y. Lu, Resonant field enhancement near bound states in the continuum on periodic structures, *Phys. Rev. A* **101**, 043825 (2020).
- [11] S. Joseph, S. Pandey, S. Sarkar, and J. Joseph, Bound states in the continuum in resonant nanostructures: An overview of engineered materials for tailored applications, *Nanophotonics* **10**, 4175 (2021).
- [12] K. Koshelev, Z. Sadrieva, A. Shcherbakov, Y. Kivshar, and A. Bogdanov, Bound states of the continuum in photonic structures, *Phys. Usp.* **66**, 494 (2021).
- [13] P. Hu, C. Xie, Q. Song, A. Chen, H. Xiang, D. Han, and J. Zi, Bound states in the continuum based on the total internal reflection of Bloch waves, *Natl. Sci. Rev.* **10**, nwac043 (2023).
- [14] C. W. Hsu, B. Zhen, J. Lee, S. G. Johnson, J. D. Joannopoulos, and M. Soljačić, Observation of trapped light within the radiation continuum, *Nature (London)* **499**, 188 (2013).
- [15] E. N. Bulgakov and A. F. Sadreev, Bound states in the continuum with high orbital angular momentum in a dielectric rod with periodically modulated permittivity, *Phys. Rev. A* **96**, 013841 (2017).
- [16] K. Koshelev, G. Favraud, A. Bogdanov, Y. Kivshar, and A. Fratallocchi, Nonradiating photonics with resonant dielectric nanostructures, *Nanophotonics* **8**, 725 (2019).
- [17] A. Taghizadeh and I.-S. Chung, Quasi bound states in the continuum with few unit cells of photonic crystal slab, *Appl. Phys. Lett.* **111**, 031114 (2017).
- [18] E. Bulgakov and A. Sadreev, Propagating Bloch bound states with orbital angular momentum above the light line in the array of dielectric spheres, *J. Opt. Soc. Am. A* **34**, 949 (2017).
- [19] Z. F. Sadrieva, M. A. Belyakov, M. A. Balezin, P. V. Kapitanova, E. A. Nenasheva, A. F. Sadreev, and A. A. Bogdanov, Experimental observation of a symmetry-protected bound state in the continuum in a chain of dielectric disks, *Phys. Rev. A* **99**, 053804 (2019).
- [20] I. Y. Polishchuk, A. A. Anastasiev, E. A. Tsyvkunova, M. I. Gozman, S. V. Solov'ov, and Y. I. Polishchuk, Guided modes in the plane array of optical waveguides, *Phys. Rev. A* **95**, 053847 (2017).
- [21] M. S. Sidorenko, O. N. Sergaeva, Z. F. Sadrieva, C. Roques-Carnes, P. S. Muraev, D. N. Maksimov, and A. A. Bogdanov, Observation of an Accidental Bound State in the Continuum in a Chain of Dielectric Disks, *Phys. Rev. Applied* **15**, 034041 (2021).
- [22] Z. Zhang, E. Bulgakov, K. Pichugin, A. Sadreev, Y. Xu, and Y. Qin, Super Quasibound State in the Continuum, *Phys. Rev. Applied* **20**, L0011003 (2023).
- [23] L. Ni, J. Jin, C. Peng, and Z. Li, Analytical and statistical investigation on structural fluctuations induced radiation in photonic crystal slabs, *Opt. Express* **25**, 5580 (2017).
- [24] E. E. Maslova, M. V. Rybin, A. A. Bogdanov, and Z. F. Sadrieva, Bound states in the continuum in periodic structures with structural disorder, *Nanophotonics* **10**, 4313 (2021).
- [25] J. Jin, X. Yin, L. Ni, M. Soljačić, B. Zhen, and C. Peng, Topologically enabled ultrahigh- Q guided resonances robust to out-of-plane scattering, *Nature (London)* **574**, 501 (2019).
- [26] M.-S. Hwang, H.-C. Lee, K.-H. Kim, K.-Y. Jeong, S.-H. Kwon, K. Koshelev, Y. Kivshar, and H.-G. Park, Ultralow-threshold laser using super-bound states in the continuum, *Nat. Commun.* **12**, 4135 (2021).
- [27] M. Kang, S. Zhang, M. Xiao, and H. Xu, Merging Bound States in the Continuum at Off-High Symmetry Points, *Phys. Rev. Lett.* **126**, 117402 (2021).
- [28] E. Bulgakov, A. Pilipchuk, and A. Sadreev, Desktop laboratory of bound states in the continuum in metallic waveguide with dielectric cavities, *Phys. Rev. B* **106**, 075304 (2022).
- [29] L. Huang, B. Jia, Y. K. Chiang, S. Huang, C. Shen, F. Deng, T. Yang, D. A. Powell, Y. Li, and A. E. Miroshnichenko, Topological supercavity resonances in the finite system, *Adv. Sci.* **9**, 2200257 (2022).
- [30] L. Huang, L. Xu, D. A. Powell, W. J. Padilla, and A. E. Miroshnichenko, Resonant leaky modes in all-dielectric

- metasystems: Fundamentals and applications, *Phys. Rep.* **1008**, 1 (2023).
- [31] K. Wang, H. Liu, Z. Li, M. Liu, Y. Zhang, and H. Zhang, All-dielectric metasurface-based multimode sensing with symmetry-protected and accidental bound states in the continuum, *Results Phys.* **46**, 106276 (2023).
- [32] N. M. Shubin, Algebraic approach to annihilation and repulsion of bound states in the continuum in finite systems, *J. Math. Phys.* **64**, 042103 (2023).
- [33] H. Barkaoui, K. Du, Y. Chen, S. Xiao, and Q. Song, Merged bound states in the continuum for giant superchiral field and chiral mode splitting, *Phys. Rev. B* **107**, 045305 (2023).
- [34] J. Fan, Z. Xue, H. Xing, D. Lu, G. Xu, J. Gu, J. Han, and L. Cong, Hybrid bound states in the continuum in terahertz metasurfaces, [arXiv:2303.12264v1](https://arxiv.org/abs/2303.12264v1).
- [35] H. Zhang, W. Zhang, S. Chen, P. Duan, J. Li, L. Shi, J. Zi, and X. Zhang, Experimental observation of vector bound states in the continuum, *Adv. Opt. Mater.* **11**, 2203118 (2023).
- [36] H. Qin, Z. Su, M. Liu, Y. Zeng, M.-C. Tang, M. Li, Y. Shi, W. Huang, C.-W. Qiu, and Q. Song, Arbitrarily polarized bound states in the continuum with twisted photonic crystal slabs, *Light: Sci. Appl.* **12**, 66 (2023).
- [37] K. Koshelev and Y. Kivshar, Light trapping gets a boost, *Nature (London)* **574**, 491 (2019).
- [38] L. Yuan and Y. Y. Lu, Perturbation theories for symmetry-protected bound states in the continuum on two-dimensional periodic structures, *Phys. Rev. A* **101**, 043827 (2020).
- [39] J. Wiersig, Formation of Long-Lived, Scarlike Modes near Avoided Resonance Crossings in Optical Microcavities, *Phys. Rev. Lett.* **97**, 253901 (2006).
- [40] Q. H. Song and H. Cao, Improving Optical Confinement in Nanostructures via External Mode Coupling, *Phys. Rev. Lett.* **105**, 053902 (2010).
- [41] M. V. Rybin, K. L. Koshelev, Z. F. Sadrieva, K. B. Samusev, A. A. Bogdanov, M. F. Limonov, and Y. S. Kivshar, High-Q Supercavity Modes in Subwavelength Dielectric Resonators, *Phys. Rev. Lett.* **119**, 243901 (2017).
- [42] W. Chen, Y. Chen, and W. Liu, Multipolar conversion induced subwavelength high-q kerker supermodes with unidirectional radiations, *Laser Photonics Rev.* **13**, 1900067 (2019).
- [43] W. Wang, L. Zheng, L. Xiong, J. Qi, and B. Li, High Q-factor multiple Fano resonances for high-sensitivity sensing in all-dielectric metamaterials, *OSA Continuum* **2**, 2818 (2019).
- [44] M. Odit, K. Koshelev, S. Gladyshev, K. Ladutenko, Y. Kivshar, and A. Bogdanov, Observation of supercavity modes in subwavelength dielectric resonators, *Adv. Mater.* **33**, 2003804 (2020).
- [45] I. Volkovskaya, L. Xu, L. Huang, A. I. Smirnov, A. E. Miroshnichenko, and D. Smirnova, Multipolar second-harmonic generation from high-Q quasi-BIC states in subwavelength resonators, *Nanophotonics* **9**, 3953 (2020).
- [46] L. Huang, L. Xu, M. Rahmani, D. N. Neshev, and A. E. Miroshnichenko, Pushing the limit of high-Q mode of a single dielectric nanocavity, *Adv. Photonics* **3**, 016004 (2021).
- [47] E. N. Bulgakov and A. F. Sadreev, Bloch bound states in the radiation continuum in a periodic array of dielectric rods, *Phys. Rev. A* **90**, 053801 (2014).
- [48] Z. Huand Y. Y. Lu, Standing waves on two-dimensional periodic dielectric waveguides, *J. Optics* **17**, 065601 (2015).
- [49] P. Vincent and M. Neviere, Corrugated dielectric waveguides: A numerical study of the second-order stop bands, *Appl. Phys.* **20**, 345 (1979).
- [50] Y. Yang, C. Peng, Y. Liang, Z. Li, and S. Noda, Analytical Perspective for Bound States in the Continuum in Photonic Crystal Slabs, *Phys. Rev. Lett.* **113**, 037401 (2014).
- [51] D. A. Bykov and L. L. Doskolovich, $\omega - kx$ Fano line shape in photonic crystal slabs, *Phys. Rev. A* **92**, 013845 (2015).
- [52] X. Gao, C. W. Hsu, B. Zhen, X. Lin, J. D. Joannopoulos, M. Soljačić, and H. Chen, Formation mechanism of guided resonances and bound states in the continuum in photonic crystal slabs, *Sci. Rep.* **6**, 31908 (2016).
- [53] L. Ni, Z. Wang, C. Peng, and Z. Li, Tunable optical bound states in the continuum beyond in-plane symmetry protection, *Phys. Rev. B* **94**, 245148 (2016).
- [54] H. Friedrich and D. Wintgen, Interfering resonances and bound states in the continuum, *Phys. Rev. A* **32**, 3231 (1985).
- [55] A. Volya and V. Zelevinsky, Non-Hermitian effective Hamiltonian and continuum shell model, *Phys. Rev. C* **67**, 054322 (2003).
- [56] A. Sadreev, Interference traps waves in an open system: Bound states in the continuum, *Rep. Prog. Phys.* **84**, 055901 (2021).
- [57] R. Kikkawa, M. Nishida, and Y. Kadoya, Polarization-based branch selection of bound states in the continuum in dielectric waveguide modes anti-crossed by a metal grating, *New J. Phys.* **21**, 113020 (2019).
- [58] S. Gladyshev, A. Shalev, K. Frizyuk, K. Ladutenko, and A. Bogdanov, Bound states in the continuum in multipolar lattices, *Phys. Rev. B* **105**, L241301 (2022).
- [59] K. Yasumoto and H. Jia, Modeling of photonic crystals by multilayered periodic arrays of circular cylinders, in *Electromagnetic Theory and Applications for Photonic Crystals*, edited by K. Yasumoto (MIT Press, Cambridge, MA, 2006), p. 135, Eq. (3.50).
- [60] S. G. Johnson, S. Fan, A. Mekis, and J. D. Joannopoulos, Multipole-cancellation mechanism for high-Q cavities in the absence of a complete photonic band gap, *Appl. Phys. Lett.* **78**, 3388 (2001).
- [61] G. Blaustein, M. Gozman, O. Samoylova, I. Polishchuk, and A. Burin, Guiding optical modes in chains of dielectric particles, *Opt. Express* **15**, 17380 (2007).
- [62] A. Asenjo-Garcia, M. Moreno-Cardoner, A. Albrecht, H. J. Kimble, and D. E. Chang, Exponential Improvement in Photon Storage Fidelities Using Subradiance and “Selective Radiance” in Atomic Arrays, *Phys. Rev. X* **7**, 031024 (2017).
- [63] E. N. Bulgakov and A. F. Sadreev, High-Q resonant modes in a finite array of dielectric particles, *Phys. Rev. A* **99**, 033851 (2019).
- [64] Y. Zhang, I. Bulu, W.-M. Tam, B. Levitt, J. Shah, T. Botto, and M. Loncar, High-Q/V air-mode photonic crystal cavities at microwave frequencies, *Opt. Express* **19**, 9371 (2011).

- [65] C. Ciminelli, D. Conteduca, F. Dell’Olio, and M. N. Armenise, Design of an optical trapping device based on an ultra-high q/v resonant structure, *IEEE Photonics J.* **6**, 0600916 (2014).
- [66] S. Han and Y. Shi, Systematic analysis of optical gradient force in photonic crystal nanobeam cavities, *Opt. Express* **24**, 452 (2016).
- [67] S. Hu, M. Khater, R. Salas-Montiel, E. Kratschmer, S. Engelmann, W. M. J. Green, and S. M. Weiss, Experimental realization of deep-subwavelength confinement in dielectric optical resonators, *Sci. Adv.* **4**, aat2355 (2018).
- [68] D. F. Kornovan, R. S. Savelev, Y. Kivshar, and M. I. Petrov, High- Q localized states in finite arrays of subwavelength resonators, *ACS Photonics* **8**, 3627 (2021).
- [69] X. Qi, J. Wu, F. Wu, M. Ren, Q. Wei, Y. Wang, H. Jiang, Y. Li, Z. Guo, Y. Yang, W. Zheng, Y. Sun, and H. Chen, Steerable merging bound states in the continuum on a quasi-flatband of photonic crystal slabs without breaking symmetry, *Photonics Research* **11**, 1262 (2023).
- [70] R. Kikkawa, M. Nishida, and Y. Kadoya, Bound states in the continuum and exceptional points in dielectric waveguide equipped with a metal grating, *New J. Phys.* **22**, 073029 (2020).